

Multi-Generational Black Hole Population Analysis with an Astrophysically Informed Mass Function

Yannick Ulrich,^{1,2,*} Djuna Croon,^{1,†} Jeremy Sakstein,^{3,‡} and Samuel D. McDermott^{4,§}

¹*Institute for Particle Physics Phenomenology, Department of Physics, Durham University, Durham DH1 3LE, U.K.*

²*Institut für Theoretische Physik & AEC, Universität Bern, Sidlerstrasse 5, CH-3012 Bern, Switzerland*

³*Department of Physics & Astronomy, University of Hawai'i,
Watanabe Hall, 2505 Correa Road, Honolulu, HI, 96822, USA*

⁴*Department of Astronomy and Astrophysics, University of Chicago, Chicago, IL, USA*

(Dated: June 11, 2024)

We analyze the population statistics of black holes in the LIGO/Virgo/KAGRA GWTC-3 catalog using a parametric mass function derived from simulations of massive stars experiencing pulsational pair-instability supernovae (PPISN). Our formalism enables us to separate the black hole mass function into sub-populations corresponding to mergers between objects formed via different astrophysical pathways, allowing us to infer the properties of black holes formed from stellar collapse and black holes formed via prior mergers separately. Applying this formalism, we find that this model fits the data better than the powerlaw+peak model with Bayes factor 9.7 ± 0.1 . We measure the location of the lower edge of the upper black hole mass gap to be $M_{\text{BHMG}} = 84.05^{+17.19}_{-12.88} M_{\odot}$, providing evidence that the $35 M_{\odot}$ Gaussian peak detected in the data using other models is not associated with the PPISN pile-up predicted to precede this gap. Incorporating spin, we find that the normalized spins of stellar remnant black holes are close to zero while those of higher generation black holes tend to larger values. All of these results are in accordance with the predictions of stellar structure theory and black hole merger scenarios. Finally, we combine our mass function with the spectral siren method for measuring the Hubble constant to find $H_0 = 36.19^{+7.50}_{-10.91}$ km/s/Mpc and discuss potential explanations of this low value. Our results demonstrate how astrophysically-informed mass functions can facilitate the interpretation of gravitational wave catalog data to provide information about black hole formation and cosmology. Future data releases will improve the precision of our measurements.

I. INTRODUCTION

The LIGO/Virgo/KAGRA (LVK) gravitational wave interferometers have observed around 100 binary black hole mergers, documented in their most recent GWTC-3 catalog [1]. Inferring the population statistics of the masses, spins, eccentricities, and alignment of these objects provides insights into how they formed. Interpreting the data in the context of the underlying physics requires knowledge of the black hole mass function (BHMF), which is presently unknown due to the difficulty in predicting it from first principles. The majority of objects observed by LVK are expected to be *first-generation* black holes (BHs) formed from the collapse of massive stars ($M \gtrsim 20 M_{\odot}$), but some fraction may be *second generation* black holes (or higher-generation) that formed from the merger of two first generation objects. By fitting parameterized BHMFs to the data, the physics underlying the formation of these diverse populations can be inferred. The free parameters in the BHMFs provide measurable constraints on the formation processes.

Another application of BHMFs is to measure cosmological parameters via the *spectral sirens* method. LVK

measures the detector frame masses of each black hole and the luminosity distance to the merger, but the redshift is unknown. Features in the BHMF break the degeneracy between redshift and source-frame mass, enabling measurements of various cosmological parameters. Of these, the Hubble constant H_0 is best-constrained using this method, but the measured value is highly-sensitive to the assumed BHMF [2].

In reference [3], three of us proposed a novel BHMF which models the physics of pair-instability supernovae with three free parameters. This mass function was designed to capture the physics of pulsational pair instability supernovae (PPISN), which predicts an *upper black hole mass gap* (BHMG) — a discontinuity in the black hole mass distribution preceded by a peak due to PPISN pile-up. Bayesian analysis of the GWTC-2 catalog with this mass function resulted in mass gap $M_{\text{BHMG}} = 55.4^{+3.0}_{-6.1} M_{\odot}$, compatible with the expectation from stellar structure theory. The higher-generation BHs that *pollute* the gap were modeled as a single additional background; spin and luminosity distance information was not used, and, aligned with conventions in the field, only the heaviest black hole in each merger event (the “primary”) was fit using the mass function.

Continuing this program connecting theory with observation, in this work we extend the formalism and analysis in [3] on multiple fronts. First, we include the secondary objects; and introduce additional components to the BHMF corresponding to higher-generation BHs. This enables us to constrain the fraction of merger events that

* yannick.ulrich@cern.ch

† djuna.l.croon@durham.ac.uk

‡ sakstein@hawaii.edu

§ samueldmcdermott@gmail.com

contain a higher-generation BH. Second, we incorporate spin information, which we use this to measure the spin of first-generation (1g) and second-generation (2g) BHs separately. Finally, we include luminosity distance information to measure the Hubble constant using the spectral sirens method.

A summary of our key results is as follows:

- Our PPISN-inspired BHMF is preferred over the phenomenological power law+peak model with Bayes factor $\log Z_{\text{PPISN}} - \log Z_{\text{PLP}} = 9.7 \pm 0.1$.
- We measure the location of the upper BHMG to be $M_{\text{BHMG}} = 84.05_{-12.88}^{+17.19} M_{\odot}$, larger than previous measurements but consistent with stellar structure theory. This provides evidence that the $35M_{\odot}$ peak present in the data is not associated with the PPISN pile-up.
- The dimensionless spin parameter distribution of first-generation BHs is peaked close to zero while the distribution of the higher-generation population prefers larger values. This is in accordance with stellar structure theory and dynamical merger scenarios.
- We measure $H_0 = 36.19_{-10.91}^{+17.50}$ km/s/Mpc, smaller than previous studies and discrepant with astrophysical and cosmological measurements at the $\sim 2\sigma$ level.

We discuss these findings and their origin in detail below.

This paper is organized as follows. In Section II we introduce the mass and spin functions we use in our data analysis, and describe the spectral sirens method for measuring H_0 . In Section III we describe our data analysis. Our results are presented in Section IV. We discuss these results and conclude in Section V.

II. POPULATION MODELING

A. Mass function

In what follows we assume the primary and secondary black holes are picked from identical mass distributions, and that the different generations of black holes are represented by different mass distributions. This implies, using the chain rule of probability, that the total probability distribution is given by

$$\begin{aligned} \mathbb{P}(\vec{\omega}|\vec{\theta}) \propto & p^{(1g)}(M_1|\vec{\theta})p^{(1g)}(M_2|\vec{\theta})f(q;\beta_q^{(1)}) \\ & + \lambda_{12}p^{(1g)}(M_1|\vec{\theta})p^{(2g)}(M_2|\vec{\theta})f(q;\beta_q^{(2)}) \\ & + \lambda_{21}p^{(2g)}(M_1|\vec{\theta})p^{(1g)}(M_2|\vec{\theta})f(q;\beta_q^{(2)}) + \dots \end{aligned} \quad (1)$$

where $p^{(ng)} = \frac{dN^{(ng)}}{dM}$ is the underlying mass function of the n^{th} generation black holes. Thus, the different terms account for BH binaries formed from a stellar binary, and BH binaries which include a higher generation BH. We assume that the primary formation channel for BBH mergers is from stellar collapse, implying that the

first-generation black holes dominate the mass function. In (1), the function f accounts for a preferential formation mechanism for binaries with a particular mass ratio $q \equiv M_2/M_1$. Following [4], we choose $f = q^{\beta_q}$. We allow for different β_q between binaries formed of two first generation black holes.

The mass function we use for the first generation black holes is [3]

$$p^{(1g)} \propto M_{\text{BH}}^b \left[1 + \frac{2a^2 M_{\text{BH}}^{1/2} (M_{\text{BHMG}} - M_{\text{BH}})^{a-1}}{M_{\text{BHMG}}^{a-1/2}} \right] \times S(M_{\text{BH}}|M_{\text{min}}, \delta_m) \quad (2)$$

with “turn-on” function at the low mass end,

$$S(x|y, z) = \left[\exp\left(\frac{z}{x-y} + \frac{z}{x-y-z}\right) + 1 \right]^{-1}, \quad (3)$$

$$\int_y^{y+z} dx S(x|y, z) = \frac{z}{2}$$

for black holes in the range $M_{\text{min}} \leq M_{\text{BH}} \leq M_{\text{min}} + \delta_m$, and $S = 0(1)$ for $M_{\text{BH}} < M_{\text{min}}$ ($M_{\text{BH}} > M_{\text{min}} + \delta_m$), following the analysis in [5]. This mass function was derived from one-dimensional stellar structure simulations of stellar collapse to black holes and incorporates the effects of PPISN. Reference [3] found that this was a good fit to the BHMF for a wide range of uncertain stellar parameters e.g., nuclear reaction rates. The parameter M_{BHMG} corresponds to the location of the BHMG, the parameter a measures the width of the black hole mass spectrum (final BH mass vs. initial BH mass), and the parameter b measures a combination of the slope of the initial mass function (IMF) and the zero-age main-sequence to zero-age helium burning transfer function. Note that this function diverges at $M = M_{\text{BHMG}}$, forcing the peak in the black hole mass spectrum (the heaviest BH formed from stellar collapse) to correspond to the location of the upper BHMG. See [3] for more details.

We further assume that the higher generation black holes are increasingly rarer and that binary formation mechanisms for black holes from the same generation are not more efficient than cross-generational coupling. We therefore expect a hierarchy in λ_{ij} parameters where $1 > \lambda_{21} > \lambda_{12} > \dots$. We will ignore third-order and higher generations in the following so we only need to include a distribution for the second-generation black holes. As in [3], we use

$$p^{(2g)} = S(M_{\text{BH}}|\text{min}, \delta_m) \begin{cases} 1 & m < m_{2g \text{ min}} \\ \left(\frac{m}{M_{\text{BHMG}} + M_{\text{min}} + \delta_m/2}\right)^d & m \geq m_{2g \text{ min}} \end{cases} \quad (4)$$

where $m_{2g \text{ min}} = M_{\text{BHMG}} + M_{\text{min}} + \frac{\delta_m}{2}$. This approximates the secondary mass function found in Figure 5 of [3] in the absence of mass- and environment-dependent binary formation efficiency effects. We will explicitly verify that our assumption $\lambda_{ij} \ll 1$ is satisfied *a posteriori*.

The λ s in (1) are a measure of the number black holes in each population, provided that the different contributions to (1) are appropriately normalised. To be precise, we write

$$\lambda_{12} = \frac{N(2 \in 2g)}{N_{\text{tot}}} \quad \text{and} \quad \lambda_{21} = \frac{N(1 \in 2g)}{N_{\text{tot}}}, \quad (5)$$

where $N(i \in 2g) \equiv N_i$ counts the number of primary ($i = 1$) and secondary ($i = 2$) black holes in the second generation. To avoid the dependence on N_{tot} we similarly introduce N_0 that counts the number of events with both black holes being first generation. With this, we now need to calculate the following normalisation integrals

$$\begin{aligned} \frac{N_{\text{tot}}}{N_0} &= \int_0^\infty dm_1 \int_0^{m_1} dm_2 p^{(1g)}(M_1|\vec{\theta})p^{(1g)}(M_2|\vec{\theta})f(q; \beta_q^{(1)}) \\ \frac{N_{\text{tot}}}{N_1} &= \int_0^\infty dm_1 \int_0^{m_1} dm_2 p^{(1g)}(M_1|\vec{\theta})p^{(2g)}(M_2|\vec{\theta})f(q; \beta_q^{(2)}) \\ \frac{N_{\text{tot}}}{N_2} &= \int_0^\infty dm_1 \int_0^{m_1} dm_2 p^{(2g)}(M_1|\vec{\theta})p^{(1g)}(M_2|\vec{\theta})f(q; \beta_q^{(2)}) \end{aligned} \quad (6)$$

These integrals can be split into terms that can be calculated analytically in terms of hypergeometric functions and those that involve the smoothing function S which cannot be analytically integrated. The five remaining integrals (three one dimensional and two dimensional ones) are evaluated numerically over a fine grid as part of the inference process. We have provided a machine-readable version of these integrals as an ancillary file to this submission¹ [6].

We will compare our mass function to the phenomenological power law+peak (PLP) mass function introduced in [5, 7]. This mass function was also motivated by the expectation of a PPISN pile-up, and provides the best fit to the GWTC-2 and GWTC-3 of the models studied by LVK. The primary mass distribution follows,

$$\begin{aligned} p(M_1|\vec{\theta}) &= \left[(1 - \lambda_{\text{peak}})\mathfrak{P}(m_1 | -\alpha, m_{\text{max}}) \right. \\ &\quad \left. + \lambda_{\text{peak}}G(m_1 | \mu_m, \sigma_m) \right] S(m_1 | M_{\text{min}}, \delta_m). \end{aligned} \quad (7)$$

where $\mathfrak{P}(m_1 | -\alpha, m_{\text{max}})$ is a normalized power law distribution with spectral index $-\alpha$ and high-mass cut-off m_{max} , $G(m_1 | \mu_m, \sigma_m)$ is a normalized Gaussian distribution with mean μ_m and width σ_m , the parameter λ_{peak} is a mixing fraction determining the relative prevalence of mergers in \mathfrak{P} and G , and $S(m_1, M_{\text{min}}, \delta_m)$ is the ‘‘turn-on’’ function (3). While the peak in this mass function was originally inspired by PPISN, it can float freely in mass, beyond PPISN masses which have been found in stellar structure simulations.

B. Spin

When two black holes merge, their individual spins and the orbital angular momentum combine to form the spin of the new black hole. If the black holes are of equal mass and non-spinning, the resulting black hole has a spin parameter around 0.69 [8]. This value is generally consistent across mergers with nonzero spin due to the *orbital hang-up effect*. When spins align with the orbital momentum, the merger takes longer, enhancing the spin. Conversely, anti-aligned spins lead to quicker mergers and partially cancel out the spin contributions. This results in a typical spin value of about 0.7 for the remnants of prior mergers (see e.g. [9–12]).

The advantage of the use of different mass functions for the different populations in (1) is that it allows us to separate the spin distributions. Because of the effect above, black holes formed in the dynamical merger scenario should have a normalised spin magnitude tending to 0.7, whereas black holes formed in isolated stellar evolution are predicted to be born with negligible dimensionless spin magnitudes because their progenitor stars efficiently lose angular momentum to the Spruit-Tayler dynamo [13–17] (though binary evolution may change that prediction [18]). Following [5], we use β distributions for both the 1g and 2g BHs:

$$p(\chi|\alpha, \beta) \propto \chi^{\alpha-1}(1-\chi)^{\beta-1} \frac{\Gamma(\alpha+\beta)}{\Gamma(\alpha)\Gamma(\beta)} \quad (8)$$

While this does not have a physical origin, it provides a versatile distribution that can accommodate a variety of spin configurations, and is the standard in the literature.

C. Spectral Sirens

The spectral siren method can be used to make a measurement of the Hubble constant H_0 using features in the BHMF without localizing each event’s host galaxy [19, 20]. The method works by assuming an underlying BHMF. This breaks the degeneracy between BH mass and source redshift, allowing for a measurement of cosmological parameters when the latter is unknown. Unfortunately, assumptions about the source population strongly impact the determination of H_0 [21, 22]. As such, phenomenological mass functions introduce a degree of ambiguity in the determination of H_0 . Astrophysically motivated mass functions such as ours may help to remove this source of uncertainty.

To apply this method we use the detector frame masses and the luminosity distance, and solve

$$D_L(z) = \frac{(1+z)}{H_0} \int_0^z \frac{dz'}{\sqrt{\Omega_m(1+z')^3 + (1-\Omega_m)}} \quad (9)$$

to find z for each event. Note that we have assumed flat Λ CDM in Eq. (9). We then calculate the source frame

¹ <https://doi.org/10.5281/zenodo.11242245>

Mass Function (Eqs. (1), (2), and (4))	
M_{BHMG}	$[20M_{\odot}, 120M_{\odot}]$
a	$[0, +1/2]$
b	$[-4, 0]$
$\log_{10}(\lambda_{12}), \log_{10}(\lambda_{21})$	$[-7, -0.3]$
d	$[-10, 0]$
M_{min}	$[2M_{\odot}, 10M_{\odot}]$
δ_m	$[0M_{\odot}, 10M_{\odot}]$
β_q	$[-4, 12]$
Spin Distribution (Eq. (8))	
α, β	$[1, 10]$
Spectral Sirens	
H_0 (km/s/Mpc)	$[20, 150]$

TABLE I. Prior ranges for the parameters used in our data analysis.

masses from the detector frame masses as

$$m_{1,2\text{src}} = \frac{m_{1,2\text{det}}}{1+z}. \quad (10)$$

In principle, there are two free parameters, H_0 and Ω_m , but in practice Ω_m has a negligible impact on the estimate of H_0 [21] so we fix $\Omega_m = 0.308$, the best-fit value found by the Planck collaboration [23].

III. DATA ANALYSIS

We have implemented the models described in Section II into a new code: MULTIPASS — MULTI-Population Analysis of Stellar and Secondary black holes — which uses the FORTRAN library Multinest [24] to perform the Bayesian inference. Our code is available at [6] and on GitHub² The code’s modular design makes it possible to easily add new mass functions or features. Together with the code we distribute our data preparation scripts (see below) and run cards for reproducibility. We have verified that the code gives results compatible with the LVK analysis [25].

We use the injection campaign of [26] with a false-alarm rate (FAR) filter of $\text{FAR} < 1$. Similarly, we select all events up to and including GWTC-3 with $\text{FAR} < 1$ except GW170817 (a binary neutron star (BNS) merger), GW190814 (mass ratio inspiral), GW190917_114630 (includes a lower mass gap object), GW190426_152155 (large false alarm rate), GW190425 (likely BNS), and GW200115_042309 (BNS merger). This selection leaves us with 69 merger events, a detailed list of which can be found in [6].

The parameters and prior ranges we use are given in table I. In the case of the mass function, the prior ranges

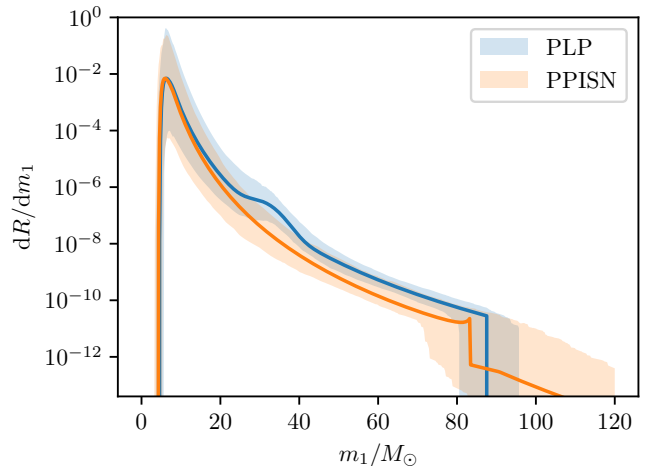


FIG. 1. 95% confidence intervals of the mass function for the primary black hole in the power law+peak model (7), and the mass function inspired by simulations of PPISN and multiple populations (1) presented here.

for the parameters in Eq. (2) are identical to those used in [3], with the parameters in the smoothing function being those chosen by LVK [5]. The spin parameters were chosen such that they allow for a broad range of distributions, including those with strong peaks. In the case of the spectral sirens analysis, we do not normalize the different mass functions $p^{(ng)}$ because the measurement on H_0 is only sensitive to features in the mass function and does not depend on the generation of each black hole. We check *a posteriori* that the hierarchy in λ_{ij} motivated above is respected such that it remains appropriate to truncate the mass function.

IV. RESULTS

A. Mass Function Analysis

The results of fitting our mass function in equation 2 to the GWTC-3 catalog (sans the events stated above) using our split-population formalism in equation (1) are shown in Figure 1 and in the corner plots in Figure 2; the best-fitting parameters are given in table II. Our mass function defined by (1), (2) and (4) provides a better fit to the data than PLP, with a Bayes evidence factor of $\log Z_{\text{PPISN}} - \log Z_{\text{PLP}} = 9.7 \pm 0.1$. The most relevant quantity is M_{BHMG} , which we measure to be $M_{\text{BHMG}} = 84.05^{+17.19}_{-12.88} M_{\odot}$. As noted above, this feature is a prediction of stellar structure theory, resulting pair-instability supernova, which prevent BHs with masses in the approximate range $50M_{\odot}$ – $120M_{\odot}$ (depending on the stellar parameters) from forming [27–29]. Currently, there is no conclusive evidence for an upper mass gap in the GWTC-3 catalog [25]. In the 1g mass function (2),

² <https://github.com/multipass-black-holes/multipass>.

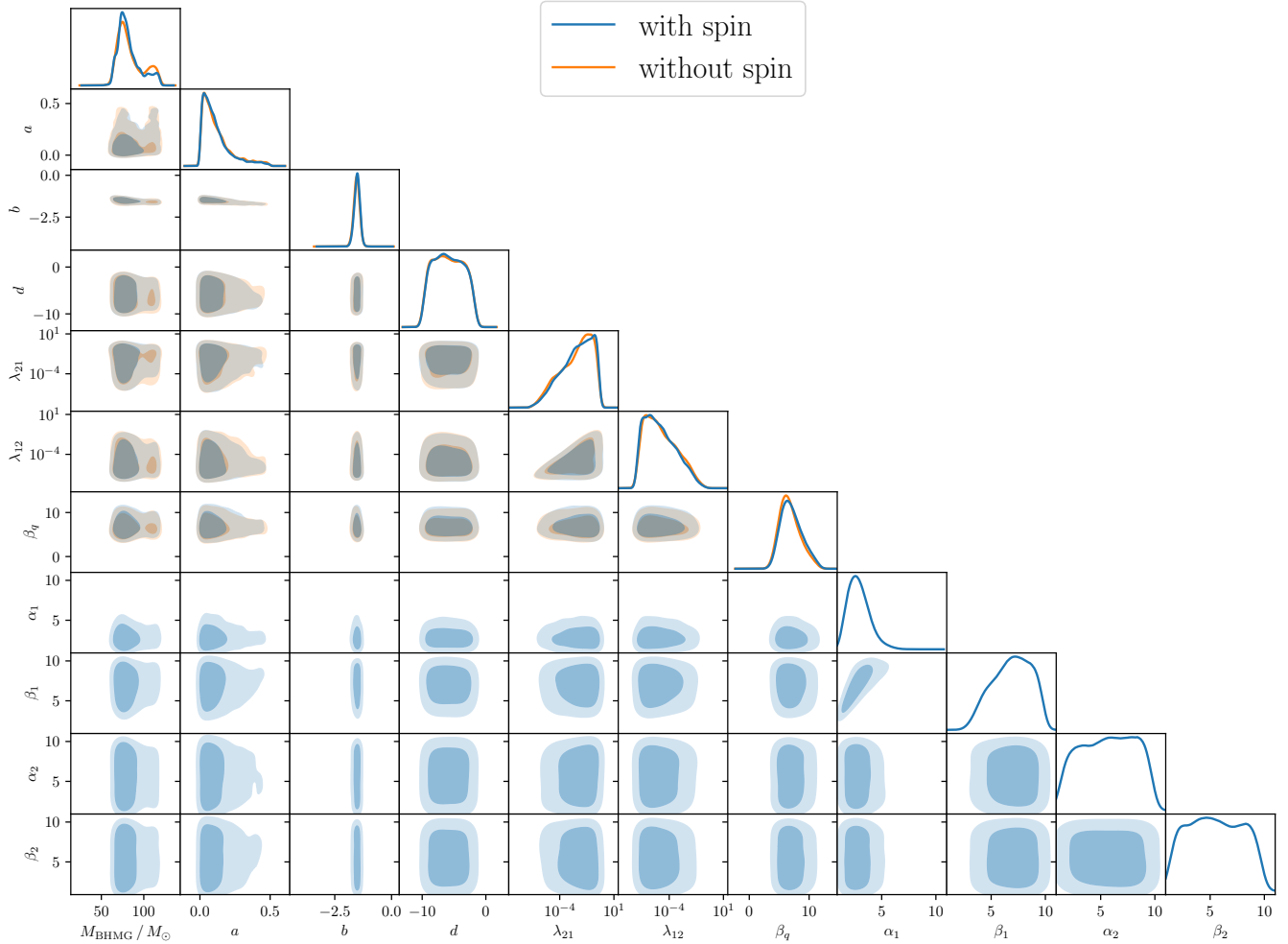


FIG. 2. Corner plot of the parameters in the mass function in equations (1), (2), and (4) in orange and the simultaneous fit of mass and spin function in blue. In orange, the fit without taking spin information into account, in blue, the fit to both mass and spin information; there is good correspondence between the mass function parameters. The variation in each parameter depicted corresponds to the prior range used in our study. Parameters of the mass function “turn-on” are not depicted, but do not correlate significantly with any of the parameters shown. For the spin parameters, subscript-1s refer to 1g BHs and subscript-2s refer to 2g BHs.

the upper mass gap feature is incorporated by virtue of being predicted by stellar structure theory and is therefore detected by design. It is possible that, when using phenomenological BHMFs that do not separate populations, this feature may be obscured by 2g mass gap *pollutants*. The posterior we find for M_{BHMG} is bimodal and weakly correlated with λ_{12} , λ_{21} . This correlation is expected because for larger M_{BHMG} , fewer black holes will be found in the higher generation population.

The posterior for b is well converged and not correlated with any of the other variables. Physically, b is an index corresponding to the slope of the number of stars that collapse to form BHs as a function of mass before accounting for PPISN. The absence of a peak in the mass function (2) could have implied a less well constrained parameter b , if a peak should be there. The fact that b is

well constrained indicates that there are a sufficient number of large-mass black holes in the first generation to resolve the power law. Conversely, the parameter d , which physically represents the power law index of the higher generation population, is less well constrained. Future catalogues with more heavy mergers are likely to improve upon this.

B. Spin Distribution

The results of fitting our spin distribution in equation (8) to the GWTC-3 catalog (excluding the events stated above) using our split-population formalism in equation (1) together with the mass functions in equations (2) and (4) are shown in Figure 3. The 1g pop-

Mass Function (Eqs. (1), (2), and (4))	
M_{BHMG}	$84.05^{+17.19}_{-12.88} M_{\odot}$
a	$0.12^{+0.13}_{-0.08}$
b	$-1.53^{+0.13}_{-0.13}$
$\log_{10} \lambda_{21}$	$-2.52^{+1.33}_{-1.59}$
$\log_{10} \lambda_{12}$	$-4.71^{+1.58}_{-1.35}$
d	$-5.86^{+2.30}_{-2.26}$
M_{mmin}	$4.02^{+1.02}_{-1.01} M_{\odot}$
δ_m	$5.25^{+2.14}_{-2.26} M_{\odot}$
β_q	$6.80^{+1.84}_{-1.59}$

TABLE II. Best fit values and error estimates of the mass function analysis.

ulation prefers smaller values of the spin parameter χ than the 2g population. As discussed above, a small spin parameter for the 1g population is predicted by stellar structure theory. The preference for larger χ for the 2g population is again in agreement with the astrophysical expectations for a dynamical merger scenario, which predicts $\chi \sim 0.7$ as also explained above.

The corresponding corner plots are shown in Figure 2. Subscript-1s refer to the β -distribution for 1g BHs and subscript-2s refer to the β -distribution for 2g BHs. It is seen that the 1g generation prefers larger values of β_1 than α_1 , which translates into a preference for small values of the spin parameter χ close to zero. The correlation between the parameters preserves this preference under variations. In contrast, the 2g population is less well constrained by virtue of the fact that fewer events fall into this category. At the peaks of their distributions, the value of α_2 is larger than β_2 , implying a preference for larger spin parameters.

C. Spectral Siren Analysis

In the top panel of Figure 4 we show the marginalized posterior probability distributions for H_0 for the two different black hole mass functions introduced above: the PLP and our astrophysically-informed scenario. The PLP model peaks at a higher value of $H_0 = 56.08^{+16.16}_{-14.43}$ km/s/Mpc compared to our model, and the width of the distribution is significantly wider. Our model peaks at $H_0 = 36.19^{+17.50}_{-10.91}$ km/s/Mpc, but has support for H_0 values up to about 75 km/s/Mpc.

In Figure 4 we also show how H_0 correlates with M_{BHMG} in the PPISN model. The model prefers larger values of M_{BHMG} and smaller values of H_0 . This correlation is explained by the fact that, since the luminosity distance and detector frame masses are observed quantities, smaller H_0 implies larger source frame masses, leading to large M_{BHMG} . The values of H_0 with 1σ uncertainties reported by the Planck [30] and SHOES [31] collaborations, which lie on the edge of the posterior in-

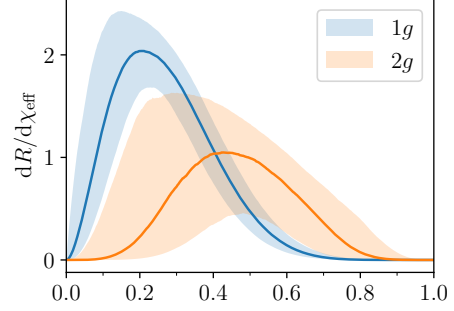


FIG. 3. 95 % confidence interval and median best fit of the spin distributions. The 1g population prefers smaller values of the dimensionless spin parameter χ than the 2g population, in agreement with astrophysical expectations.

terval, correspond to smaller values of M_{BHMG} , which is also more in line with results from stellar structure simulations. In contrast, the PLP model cuts off the mass function sharply after m_{max} . The lower masses then correspond to larger values of the inferred z and H_0 . Note that the best-fitting value of M_{BHMG} is larger than in our mass function fit in table II because that analysis used the LVK reported source frame masses, which is equivalent to fixing H_0 to a value larger than the best-fitting value found in the present analysis. The smaller best-fitting H_0 value found by allowing it to vary implies that, at fixed luminosity distance, the inferred BH masses must be larger, hence the larger value of M_{BHMG} .

V. DISCUSSION

In this study, we examined the population statistics of black holes in the LIGO/Virgo/KAGRA GWTC-3 catalog using a parametric mass function based on simulations of massive stars undergoing pulsational pair-instability supernovae. The novelty of this approach is that different sub-populations of black holes originating from either stellar collapse or previous mergers can be distinguished, enabling separate measurements of their properties and increasing the amount of information that can be extracted from the data.

Our BHMF provided a better fit to the LVK O3 data than the phenomenological power law+peak model, and we obtained a measurement of the location of the lower edge of the upper black hole mass gap: $M_{\text{BHMG}} = 84.05^{+17.19}_{-12.88} M_{\odot}$. This value differs from the $\sim 35 M_{\odot}$ peak found by more phenomenological models e.g., PLP, despite the priors allowing for such a value of M_{BHMG} . This provides evidence that the $\sim 35 M_{\odot}$ peak that appears to exist in the data with high statistical significance regardless of the method used to detect it [4, 25, 32–34] is not associated with the PPISN pile-up preceding the upper black hole mass gap. In the BHMF, this pile-up has the shape of a divergence at the location of the upper black

hole mass gap [3] rather than a peak.

The best-fit value for M_{BHMG} found in this work is notably larger than found in the analysis of GWTC-2 using the same mass function [3]. While still in the range of values found through stellar structure simulations, the current preference for a larger value is intriguing because the previous analysis focused exclusively on the primary population, which (by definition) comprises larger masses compared to the secondary population. The fact that the power law index of the 1g population b is much better constrained in the present analysis suggests that the larger catalogue allowed for a more accurate assignment of generation for large 1g-black holes. Analysis of future transient catalogues may help to elucidate the origin of the difference between GWTC-2 and GWTC-3.

Other studies found convincing evidence for the existence of a peak at $M \sim 35M_{\odot}$ in both parametric and non-parametric data analyses [4, 25, 32–34]. In future work, we plan to extend our mass function to include an astrophysically informed peak feature, in line with the motivation for this program. An example of a potential physical origin for the peak was found during the preparation of this manuscript when reference [35] discovered that, in massive stars experiencing PPISN, α -ladder burning in a range of masses exacerbates the pulsations causing more mass to be shed. The result is a pile-up whereby stars with different initial masses form BHs with near-identical final masses, giving rise to a peak in the BHMF. The location, width, and height of the peak depends upon the stellar modeling parameters, but it is possible to accommodate a feature at $35M_{\odot}$. One could then extend our formalism to include this peak using a similar procedure to the derivation of equation (2) whereby one first finds a suitable fitting function for the theoretical peak of [35] and uses this to determine the corresponding term that must be added to the BHMF. This is beyond the scope of the present work because it entails both further research on the appearance of the peak under different astrophysical circumstances and significant modifications to our formalism.

Turning to spin, our formalism enabled us to separately measure the spin distributions of stellar remnant BHs and BHs formed via prior mergers. We found that, in accordance with the predictions of stellar structure theory, the former have distributions preferring smaller values of χ while, in accordance with expectations from dynamical merger scenarios, the latter have distributions that favor larger values of χ . This result is consistent with the recent findings of [36], which also allowed for different sub-populations, but can be contrasted against the results in [25], which used the same spin model for all BH masses, and found no evidence to support or refute a trend of aligned spin with chirp mass.

Finally, we applied the spectral siren method for measuring the Hubble constant to our formalism. We found a peaked distribution at $H_0 = 36.19^{+17.50}_{-10.91}$ km/s/Mpc, discrepant with the SH0ES and Planck values at around 2σ . It is possible that this discrepancy is driven by the

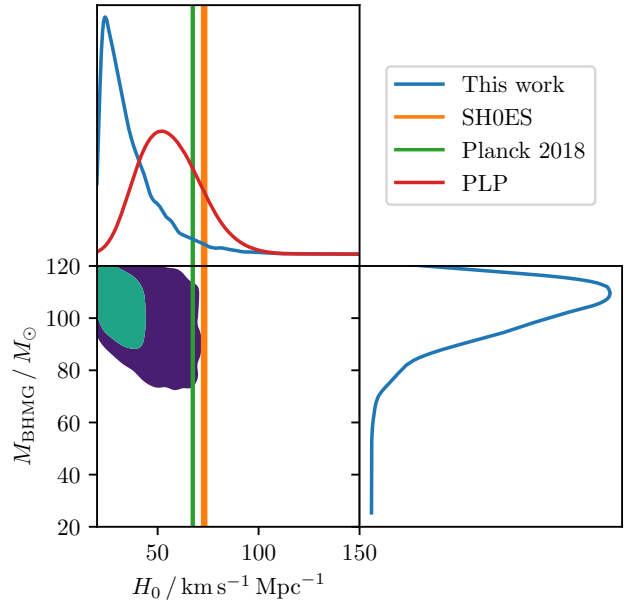


FIG. 4. Corner plot of H_0 vs. M_{BHMG} for our astrophysically-informed model (1). We include the H_0 posterior probability for the PLP model (7) and the 1σ ranges found by the SH0ES and Planck collaborations.

absence of a peak feature in our BHMF. Our BHMF is qualitatively similar to a *broken power law* model with one power given by our 1g BHMF and the second given by our 2g BHMF. Reference [22] have performed a Bayesian fit of this model in a BH sample simulated with PLP and a fiducial value of H_0 , finding that the broken power law model has a systematic bias for a smaller H_0 . The authors of [22] attribute this to the lack of any sharp features — peaks — in the model. Another possibility is that the parameters in our BHMF are redshift-dependent. For example, M_{BHMG} depends on the stellar metallicity [27], which is expected to increase with redshift. Similarly, b may be redshift-dependent because it contains information about mass loss on the red giant branch, which is also metallicity-dependent. Reference [22] also studied this effect by incorporating redshift-dependence into the location of the PLP peak, finding that the H_0 measurement is biased if redshift-dependence is not accounted for. A final potential possibility is that the fit is driven to larger M_{BHMG} because the ratio between stellar and dynamically formed black holes is redshift dependent. This implies that black holes are lighter at larger redshifts, which, in our model, would be compensated by a smaller value of H_0 . Future modifications of our formalism as described above may shed light on this issue.

VI. CONCLUSIONS

A major goal of gravitational wave astronomy is to interpret the data within the context of fundamental astrophysics. This requires connecting the black hole mass function with the predictions of stellar physics. When confronted with current data, our framework for accomplishing this, which enables separate measurements of population properties for different black hole subpopulations, yielded several results compatible with theoretical expectations. The spin distributions are compatible with a first-generation of black holes born slowly rotating from the collapse of massive stars, and a smaller second-generation of rapidly rotating BHs formed from the mergers of first-generation objects. Additionally, we obtained a measurement of the location of the upper edge of the black hole mass gap consistent with the predictions of stellar structure theory. Its location does not coincide with the $35M_{\odot}$ peak observed in the data, providing evidence that this peak is not associated with a mass gap. Our model is preferred over the canonical LIGO/Virgo/KAGRA power law+peak model, but the value for H_0 we measure is discrepant with the SH0ES

and Planck measurements at a level of 2σ , suggesting that our model may be incomplete. We suggested follow-up investigations to understand the origins of this.

SOFTWARE

Multinest 3.12 (cc616c1), Getdist 1.4.7, Astropy 5.3.4, Matplotlib 3.8.0, Numpy 1.26.1, Scipy 1.11.3, h5py 3.9.0

ACKNOWLEDGEMENTS

We thank Eric Baxter and Reed Essick for useful discussions. DC is supported by the STFC under Grant No. ST/T001011/1. This material is based upon work supported by the National Science Foundation under Grant No. 2207880. Our simulations were run on the University of Hawai'i's high-performance supercomputer KOA. The technical support and advanced computing resources from University of Hawai'i Information Technology Services – Cyberinfrastructure, funded in part by the National Science Foundation MRI award #1920304, are gratefully acknowledged.

-
- [1] R. Abbott *et al.* (LIGO Scientific, VIRGO, KAGRA), (2021), arXiv:2111.03606 [gr-qc].
 - [2] G. Pierra, in *58th Rencontres de Moriond on QCD and High Energy Interactions* (2024) arXiv:2405.17161 [gr-qc].
 - [3] E. J. Baxter, D. Croon, S. D. McDermott, and J. Sakstein, *Astrophys. J. Lett.* **916**, L16 (2021), arXiv:2104.02685 [astro-ph.CO].
 - [4] A. M. Farah, M. Fishbach, and D. E. Holz, (2023), arXiv:2308.05102 [astro-ph.HE].
 - [5] R. Abbott *et al.* (LIGO Scientific, Virgo), *Astrophys. J. Lett.* **913**, L7 (2021), arXiv:2010.14533 [astro-ph.HE].
 - [6] Y. Ulrich, D. Croon, J. Sakstein, and S. McDermott, (2024), 10.5281/zenodo.11242245.
 - [7] B. P. Abbott *et al.* (LIGO Scientific, Virgo), *Astrophys. J. Lett.* **882**, L24 (2019), arXiv:1811.12940 [astro-ph.HE].
 - [8] F. Pretorius, *Phys. Rev. Lett.* **95**, 121101 (2005), arXiv:gr-qc/0507014.
 - [9] E. Berti and M. Volonteri, *Astrophys. J.* **684**, 822 (2008), arXiv:0802.0025 [astro-ph].
 - [10] D. Gerosa and E. Berti, *Phys. Rev. D* **95**, 124046 (2017), arXiv:1703.06223 [gr-qc].
 - [11] M. Fishbach, D. E. Holz, and B. Farr, *Astrophys. J. Lett.* **840**, L24 (2017), arXiv:1703.06869 [astro-ph.HE].
 - [12] J. T. Galvez Ghera and L. C. Stein, *Class. Quant. Grav.* **38**, 045012 (2021), arXiv:2007.11578 [gr-qc].
 - [13] H. C. Spruit, *A&A* **349**, 189 (1999), arXiv:astro-ph/9907138 [astro-ph].
 - [14] H. C. Spruit, *A&A* **381**, 923 (2002), arXiv:astro-ph/0108207 [astro-ph].
 - [15] J. Fuller, A. L. Piro, and A. S. Jermyn, *MNRAS* **485**, 3661 (2019), arXiv:1902.08227 [astro-ph.SR].
 - [16] J. Fuller and L. Ma, *Astrophys. J. Lett.* **881**, L1 (2019), arXiv:1907.03714 [astro-ph.SR].
 - [17] P. Marchant and T. Moriya, (2020), arXiv:2007.06220 [astro-ph.HE].
 - [18] C. Adamcewicz, P. D. Lasky, and E. Thrane, (2023), arXiv:2311.05182 [astro-ph.HE].
 - [19] J. M. Ezquiaga, *Phys. Lett. B* **822**, 136665 (2021), arXiv:2104.05139 [astro-ph.CO].
 - [20] J. M. Ezquiaga and D. E. Holz, *Phys. Rev. Lett.* **129**, 061102 (2022), arXiv:2202.08240 [astro-ph.CO].
 - [21] S. Mastrogiovanni, K. Leyde, C. Karathanasis, E. Chassande-Mottin, D. A. Steer, J. Gair, A. Ghosh, R. Gray, S. Mukherjee, and S. Rinaldi, *Phys. Rev. D* **104**, 062009 (2021), arXiv:2103.14663 [gr-qc].
 - [22] G. Pierra, S. Mastrogiovanni, S. Perriès, and M. Mapelli, *Phys. Rev. D* **109**, 083504 (2024), arXiv:2312.11627 [astro-ph.CO].
 - [23] P. A. R. Ade *et al.* (Planck), *Astron. Astrophys.* **594**, A13 (2016), arXiv:1502.01589 [astro-ph.CO].
 - [24] F. Feroz, M. P. Hobson, and M. Bridges, *Mon. Not. Roy. Astron. Soc.* **398**, 1601 (2009), arXiv:0809.3437 [astro-ph].
 - [25] R. Abbott *et al.* (LIGO Scientific, VIRGO, KAGRA), (2021), arXiv:2111.03634 [astro-ph.HE].
 - [26] L. S. Collaboration, V. Collaboration, and K. Collaboration, (2021), 10.5281/zenodo.5546676.
 - [27] R. Farmer, M. Renzo, S. de Mink, P. Marchant, and S. Justham, (2019), 10.3847/1538-4357/ab518b, arXiv:1910.12874 [astro-ph.SR].
 - [28] R. Farmer, M. Renzo, S. de Mink, M. Fishbach, and S. Justham, (2020), arXiv:2006.06678 [astro-ph.HE].
 - [29] A. K. Mehta, A. Buonanno, J. Gair, M. C. Miller, E. Farag, R. J. deBoer, M. Wiescher, and F. X. Timmes,

- Astrophys. J. **924**, 39 (2022), arXiv:2105.06366 [gr-qc].
- [30] N. Aghanim *et al.* (Planck), Astron. Astrophys. **641**, A6 (2020), [Erratum: Astron.Astrophys. 652, C4 (2021)], arXiv:1807.06209 [astro-ph.CO].
- [31] A. G. Riess *et al.*, Astrophys. J. Lett. **934**, L7 (2022), arXiv:2112.04510 [astro-ph.CO].
- [32] B. Edelman, Z. Doctor, J. Godfrey, and B. Farr, Astrophys. J. **924**, 101 (2022), arXiv:2109.06137 [astro-ph.HE].
- [33] B. Edelman, B. Farr, and Z. Doctor, Astrophys. J. **946**, 16 (2023), arXiv:2210.12834 [astro-ph.HE].
- [34] T. A. Callister and W. M. Farr, (2023), arXiv:2302.07289 [astro-ph.HE].
- [35] D. Croon and J. Sakstein, (2023), arXiv:2312.13459 [astro-ph.HE].
- [36] G. Pierra, S. Mastrogiovanni, and S. Perriès, (2024), arXiv:2406.01679 [gr-qc].